An Actuated Universal Joint using the Twisted String Actuator: Design and Experimentation

Damian Crosby, Joaquin Carrasco, *Member, IEEE,* William Heath, *Member, IEEE,* and Andrew Weightman

***Abstract*—Actuated universal joints, or equivalent joint systems, are found in a number of robotic applications, in particular mobile snake robots, snake-arm robots and robotic tails. Such joints use a variety of actuation methods, including direct drive motors, linear screw drives, cable based systems, and hydraulics/pneumatics. In this paper the authors design and create a mechanism that uses the Twisted String Actuator (TSA) in an antagonistic triad to actuate the universal joint, using orientation sensors to create a robust closed loop control system. Various experiments then defined the performance of the system. This results in a compact high performance actuation system that exploits the properties of TSA to give it various advantages over existing actuation methods.**

***Index Terms*—???**

I. Introduction

A. Actuated Universal Joint

Actuated Universal Joint (AUJ) mechanisms are found in a wide range of robotic applications, such as confined space inspection using snake-arm robots [1], highly manoeuvrable mobile snake robots [2], and biomimetic robot tails for stability [3]. All of these applications apply different constraints on the size, mass, torque requirements, and other properties. Snake-arm robots and robotic tails can reduce the mass and size of the AUJ by moving their actuators away from the AUJs and use cables to transfer the force to the joints, or use hydraulic or pneumatic actuators which tend to be lighter than equivalent electric motors, at the expense of increased mass and bulk at the base of the arm or tail.

B. Twisted String Actuator

First developed by [4] in 2010, TSA uses two or more strings between two fixtures as a linear actuator. When one fixture is rotated (typically by an electric motor), the looped string twists into a helix, decreasing the distance between them. Equation 1 calculates the distance l_s for a two string system with infinite stiffness for a given rotation angle θ_s, where l_u is the unwound length between the fixtures and r_s is half the string thickness.

$$l_s(\theta_s) = \sqrt{l_u^2 - \theta_s^2 r_s^2} \tag{1}$$

Equation 2 defines a minimum length l_{min} for a two string system which is the length at which the helix becomes completely packed and further increases in angle or decreases in length result in recursive folding into another helix, which is undesirable in most applications.

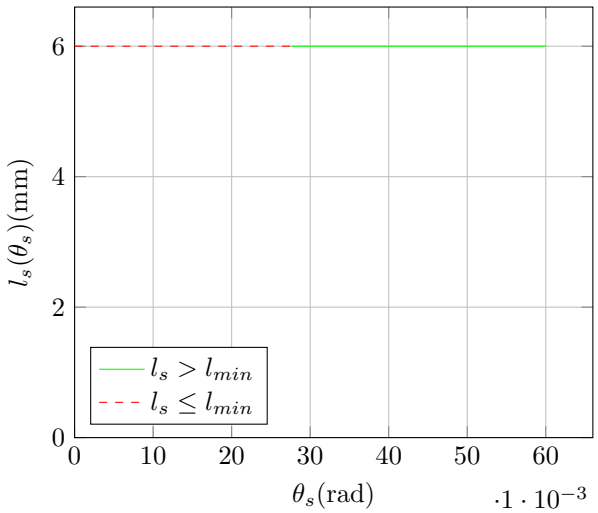

Fig. 1: Twisted String Actuator (TSA) string length against motor angle with coefficients from table I.

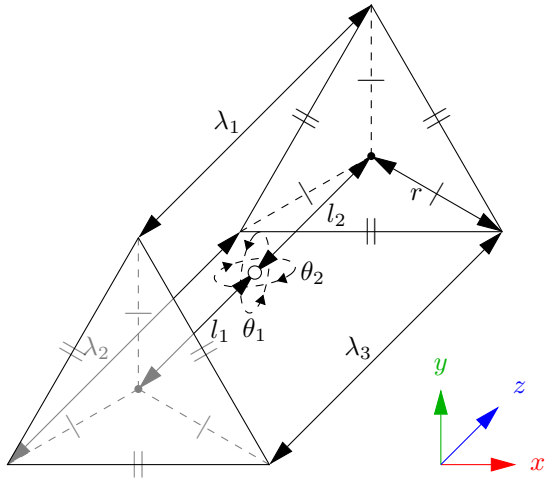

Fig. 2: Kinematic diagram of the antagonistic triad.

$$l_{min} = \frac{l_u}{\sqrt{\frac{\pi^2}{2} + 1}} \approx 0.46\ l_u \tag{2}$$

II. Antagonistic Triad

The geometric structure of the system can be described with two equilateral triangles of circumscribed radius r on two planes separated in the z axis. The centroids are then connected via a universal joint from each plane normal to

0000–0000/00$00.00 © 20XX IEEE

TABLE I: Simulation and performance estimation coefficients.

Coefficient	Value	Coefficient	Value
l_1	$45\,\mathrm{mm}$	J	$1 \times 10^{-6}\,\mathrm{kg\,m^{-2}}$
l_2	$600\,\mu\mathrm{m}$	K_L	$1000\,\mathrm{N\,m^{-1}}$
r	$13\,\mathrm{mm}$	f_{min}	$1\,\mathrm{N}$
l_n	$60\,\mathrm{mm}$	K_P	800
r_s	$200\,\mu\mathrm{m}$	K_I	5000
m	$72.619\,13\,\mathrm{g}$	K_D	50
C	$0.1315\,\mathrm{N\,mm}$	K_{P_s}	19
K_t	$0.0263\,\mathrm{N\,m\,A^{-1}}$	ω_s	$441.9\,\mathrm{rad\,s^{-1}}$
α_s	$1 \times 10^5\,\mathrm{rad\,s^{-2}}$	I_s	$0.19\,\mathrm{A}$
τ_s	$4.5\,\mathrm{mN\,m}$		

an intersecting point, described by vector $\boldsymbol{\theta} = \begin{bmatrix}\theta_1 & \theta_2\end{bmatrix}$ to denote the rotation of the second plane relative to the first, in the x and y axis around the intersecting point, and l_1 and l_2 to denote the normal distance from the intersection to the first and second plane centroids respectively. When $\boldsymbol{\theta} = \begin{bmatrix}0 & 0\end{bmatrix}$ the triangles are parallel to each other. The distance between the vertex pairs of each triangle is then denoted as $\begin{bmatrix}\lambda_1 & \lambda_2 & \lambda_3\end{bmatrix}$ for the "top", "left" and "right" vertices of the triangles. When $\boldsymbol{\theta}$ is changed, this will change λ_1, λ_2 and λ_3 respectively. A diagram of this is shown in figure 2.

To calculate the lengths of the strings for a given $\boldsymbol{\theta}$ of the AUJ, we can define a vector function $\Lambda(\boldsymbol{\theta}) = \begin{bmatrix}\lambda_1(\boldsymbol{\theta}) & \lambda_2(\boldsymbol{\theta}) & \lambda_3(\boldsymbol{\theta})\end{bmatrix}$ with l_1, l_2 and r as the coefficients, where the scalar functions are defined in equation 3.

$$\begin{aligned}
\lambda_1(\boldsymbol{\theta}) &= \sqrt{\begin{aligned}&(l_1 + l_2\cos\theta_1\cos\theta_2 + r\cos\theta_1\sin\theta_2)^2 \\ &+ (r - r\cos\theta_2 + l_2\sin\theta_2)^2 \\ &+ (l_2\cos\theta_2\sin\theta_1 + r\sin\theta_1\sin\theta_2)^2\end{aligned}} \\
\lambda_2(\boldsymbol{\theta}) &= \sqrt{(a - b + c)^2 + (l_1 - d)^2 + (e)^2} \\
\lambda_3(\boldsymbol{\theta}) &= \sqrt{(a + b - c)^2 + (l_1 + d)^2 + (e)^2}
\end{aligned} \tag{3}$$

where:

$$\begin{aligned}
a &= -\tfrac{\sqrt{3}r(\cos\theta_1 - 1)}{2} \\
b &= l_2\cos\theta_2\sin\theta_1 \\
c &= \tfrac{r\sin\theta_1\sin\theta_2}{2} \\
d &= \tfrac{\sqrt{3}r\sin\theta_1}{2} + l_2\cos\theta_1\cos\theta_2 - \tfrac{r\cos\theta_1\sin\theta_2}{2} \\
e &= \tfrac{r\cos\theta_2}{2} - \tfrac{r}{2} + l_2\sin\theta_2
\end{aligned}$$

These were simply calculated by computing the transformation matrix for each string from one end to the other in cartesian coordinates, then acquiring the Euclidean norm of the resulting translation vector $\left\|\begin{bmatrix}x_n & y_n & z_n\end{bmatrix}\right\|_2$.

III. Control System

The control system is a 4 layer cascade design, using feedback of the joint position from the accelerometers and TSA force from the load cells. It uses a second order setpoint trajectory $\boldsymbol{q}$ as input, which can either be pre-defined or generated dynamically from user input. Feedback is provided by the AUJ angular position $\boldsymbol{\theta}$, angular velocity $\dot{\boldsymbol{\theta}}$, and TSA tension force $\boldsymbol{f}$.

1) C_1 AUJ Position PID Controller
2) C_2 Inverse Dynamics
3) C_3 TSA Force Optimisation Algorithm
4) C_4 TSA Force P Controller

Functions $C_{1\ldots4}$ are then combined into a cascade function $C_4\left(C_3\left(C_2\left(C_1\left(\ldots\right),\ldots\right),\ldots\right),\ldots\right)$.

A. AUJ Position PID Controller

This function is a PID controller with the input $\boldsymbol{q}$ as the setpoint and the AUJ angular position $\boldsymbol{\theta}$ and velocity $\dot{\boldsymbol{\theta}}$ as feedback, plus the addition of a feedforward term for the input acceleration $\ddot{\boldsymbol{q}}$.

$$\begin{aligned}
\boldsymbol{\epsilon} &= \boldsymbol{q} - \boldsymbol{\theta} \\
\dot{\boldsymbol{\epsilon}} &= \dot{\boldsymbol{q}} - \dot{\boldsymbol{\theta}} \\
C_1\left(\boldsymbol{q}, \dot{\boldsymbol{q}}, \ddot{\boldsymbol{q}}, \boldsymbol{\theta}, \dot{\boldsymbol{\theta}}\right) &= K_P\boldsymbol{\epsilon} + K_I\int_0^t \boldsymbol{\epsilon}dt + K_D\dot{\boldsymbol{\epsilon}} + \ddot{\boldsymbol{q}}
\end{aligned} \tag{4}$$

In the discrete implementation used for fixed step simulation and experimental model control, the integral term is replaced by the trapezoidal rule.

$$K_I\int_0^t \boldsymbol{\epsilon} \approx \sum_{i=0}^{N} \frac{\boldsymbol{\epsilon}(t_i) + \boldsymbol{\epsilon}(t_{i-1})}{2}\Delta t \tag{5}$$

B. Inverse Dynamics

This function converts the control signal from C_1 to the desired AUJ torque using the Euler-Lagrange method in compact matrix form. Firstly the affine transformation matrix T for a coordinate frame between the AUJ pivot and the centre of mass of the follower segment can be defined. The order of R_x and R_y can be reversed, but this requires other terms to be reversed as well.

$$T(\boldsymbol{\theta}) = R_x(\theta_1)\,R_y(\theta_2)\,P_z(l_2) \tag{6}$$

Then the linear velocity jacobian J_v is simply the jacobian of the translation vector of T.

$$J_v(\boldsymbol{\theta}) = \begin{bmatrix}\frac{\partial t_{14}}{\partial\theta_1} & \frac{\partial t_{24}}{\partial\theta_1} & \frac{\partial t_{34}}{\partial\theta_1} \\ \frac{\partial t_{14}}{\partial\theta_2} & \frac{\partial t_{24}}{\partial\theta_2} & \frac{\partial t_{34}}{\partial\theta_2}\end{bmatrix} \tag{7}$$

The angular velocity jacobian J_ω is calculated using the first joint angle relative to the base frame, and the second in the frame of the first. If R_x is the first rotation in T then the first column of the jacobian is $\begin{bmatrix}100\end{bmatrix}^\intercal$ (to represent the pitch angle) and the second column is $R_x\begin{bmatrix}010\end{bmatrix}^\intercal$.

$$J_\omega(\boldsymbol{\theta}) = \begin{bmatrix}1 & r_{x_{11}} \\ 0 & r_{x_{21}} \\ 0 & r_{x_{31}}\end{bmatrix} \tag{8}$$

Then the mass matrix D can be created from the jacobians, the mass for the follower segment m and its inertia tensor $I \in \mathbb{R}^{3\times3}$, and R_x and R_y to express the inertia in the correct frame.

$$D(\boldsymbol{\theta}) = mJ_v^\intercal J_v + J_\omega^\intercal\left(R_xR_y\right)I\left(R_xR_y\right)^\intercal J_\omega^\intercal \tag{9}$$

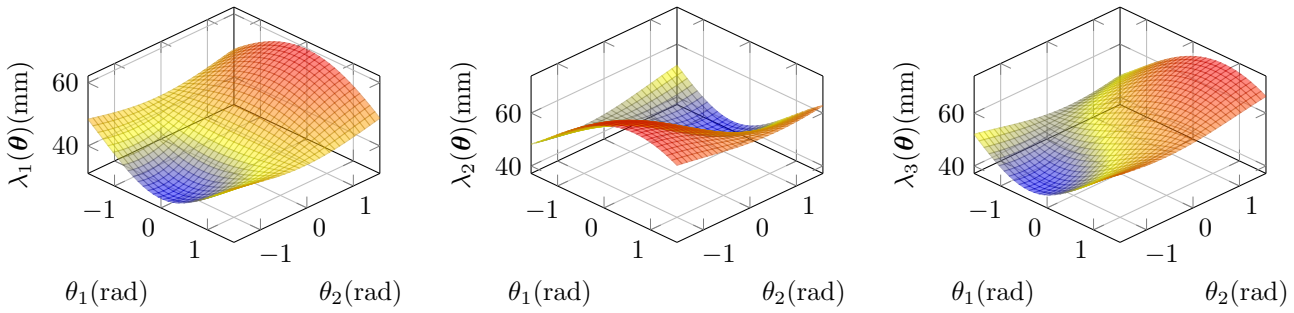

Fig. 3: Surface plots of each element of the vector function $\Lambda(\boldsymbol{\theta})$, assuming coefficient values from table I.

The centrifugal/coriolis matrix C is created from the christoffel symbols of D, along with the AUJ velocity vector $\dot{\boldsymbol{\theta}}$.

$$C\left(\boldsymbol{\theta}, \dot{\boldsymbol{\theta}}\right)_{k,j} = \sum_{i=1}^{N} \frac{1}{2} \frac{\partial d_{kj}}{\partial \theta_i} + \frac{\partial d_{ki}}{\partial \theta_j} - \frac{\partial d_{ij}}{\partial \theta_k} \dot{\theta}_i \tag{10}$$

Then the gravity term G. As the gravity vector direction is the same as the z axis as in figure 2, the height is equal to $-l_2 \cos\theta_1 \cos\theta_2$, therefore the potential energy is $mg\left(-l_2 \cos\theta_1 \cos\theta_2\right)$. The jacobian of this then becomes the gravity term.

$$G(\boldsymbol{\theta}) = \begin{bmatrix} \frac{\partial mg - l_2 \cos\theta_1 \cos\theta_2}{\partial \theta_1} \\ \frac{\partial mg - l_2 \cos\theta_1 \cos\theta_2}{\partial \theta_2} \end{bmatrix} \tag{11}$$

D, C and G are then combined to form the dynamics equation C_2, along with the AUJ position and velocity vectors. C_1 is used as the acceleration term. This results in a setpoint joint torque which can be used in the optimisation algorithm.

$$C_2\left(C_1, \boldsymbol{\theta}, \dot{\boldsymbol{\theta}}\right) = D(\boldsymbol{\theta}) C_1 + C\left(\boldsymbol{\theta}, \dot{\boldsymbol{\theta}}\right) \dot{\boldsymbol{\theta}} + G(\boldsymbol{\theta}) \tag{12}$$

C. TSA Force Optimisation Algorithm

This function uses a modified algorithm from [5] to select an optimal force vector from the desired joint torque. A force matrix F is created from the torque input C_2, jacobian J_Λ from the vector function Λ as defined in equation 3, and minimum force constant f_{min}. f_{ii} is equal to f_{min}, while the other elements in the column are based on a calculation using $J_{\Lambda_{-i,*}}$ where $-i$ is a row removed from the matrix.

$$J_\Lambda = \begin{bmatrix} \frac{\partial \lambda_1}{\partial \theta_1} & \frac{\partial \lambda_2}{\partial \theta_1} & \frac{\partial \lambda_3}{\partial \theta_1} \\ \frac{\partial \lambda_1}{\partial \theta_2} & \frac{\partial \lambda_2}{\partial \theta_2} & \frac{\partial \lambda_3}{\partial \theta_2} \end{bmatrix}$$

$$F(C_2, \boldsymbol{\theta}) = \begin{cases} f_{i,i} = f_{min} \\ f_{-i,i} = -J_{\Lambda_{-i,*}}^{-\intercal} \left(J_{\Lambda_{i,*}}^{\intercal} f_{min} + C_2 \right) \end{cases} = \begin{bmatrix} f_{min} & f_{12} & f_{13} \\ f_{21} & f_{min} & f_{23} \\ f_{31} & f_{32} & f_{min} \end{bmatrix} \tag{13}$$

Finally, the following algorithm selects one column of F to be the output force vector.

$\boldsymbol{s} \leftarrow \begin{bmatrix} \top & \top & \top \end{bmatrix}$
if $f_{23} > f_{min}$ **then** $s_2 \leftarrow \perp$ **else** $s_3 \leftarrow \perp$ **end if**
if $f_{31} > f_{min}$ **then** $s_3 \leftarrow \perp$ **else** $s_1 \leftarrow \perp$ **end if**
if $f_{12} \geq f_{min}$ **then** $s_1 \leftarrow \perp$ **else** $s_2 \leftarrow \perp$ **end if**
for $i = 1$ to 3 **do**
    if $s_i \rightarrow \top$ **then** $C_3 \leftarrow \boldsymbol{f}_{*,i}$ **end if**
end for

D. TSA Force P Controller

This function is a P controller using the measured load cell forces $\boldsymbol{f}$. The output from this can then be used to control the motor using three different control strategies implemented within the MCDC 3002 motor controller.

$$C_4(C_3, \boldsymbol{f}) = K_{P_s}(C_3 - \boldsymbol{f}) \tag{14}$$

1) Direct Current Control (DCC): This strategy corresponds to the "SOR4" mode of the MCDC 3002 []. This mode takes a preset velocity $\dot{\theta}_{set} \in [0, 4220]$ and uses a hardware PI controller with velocity feedback $\dot{\theta}_{act}$ to generate a control voltage. This voltage $\boldsymbol{V}$ is then multiplied by the signum of the result from the cascade function in order to ensure the motor spins in the right direction, and then passed to a current limiter with the current error (the result with the actual current I_{act} subtracted) as the limit, before being sent to the motor. This ensures the motor stops spinning when the target current is reached.

$$\begin{aligned} \boldsymbol{\epsilon_c} &= \dot{\theta}_{set} - \dot{\boldsymbol{\theta}}_{\boldsymbol{act}} \\ \boldsymbol{V} &= \left(K_{P_c} \boldsymbol{\epsilon_c} + K_{D_c} \int_0^t \boldsymbol{\epsilon_c} \right) \operatorname{sgn}(C_4(\ldots)) \omega(C_4(\ldots) - \boldsymbol{I_{act}}) \end{aligned} \tag{15}$$

Where $\omega(\ldots) \in [0, 1]$ is an unknown hardware limiting function that controls the motor speed depending on the current error.

2) P Current Controller: This strategy is a more direct method of current control, using a software P controller to directly set the voltage of the motor, using the MCDC 3002 as simply a passive amplifier. In this case the current error is passed directly to a P controller which has its output limited to prevent damage to the motors.

$$\boldsymbol{V} = K_{P_c} C_4(\ldots) - \boldsymbol{I_{act}} \tag{16}$$

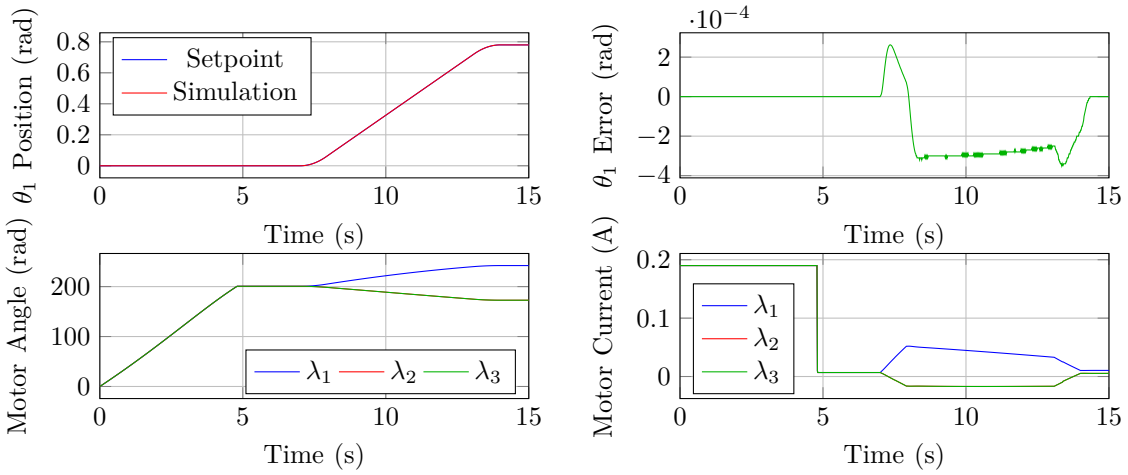

Fig. 4: Simulation results for a trajectory of θ_1 from 0 to $\frac{\pi}{4}$.

3) Velocity Control: This strategy simply uses the result from the cascade function as a velocity setpoint using the hardware velocity PI controller as in the **Direct Current Control!** (**Direct Current Control!**).

$$\boldsymbol{V} = K_{P_c}\boldsymbol{\epsilon_c} + K_{D_c}\int_0^t \boldsymbol{\epsilon_c} \tag{17}$$

IV. Simulation Results

To design and refine the parameters of the control system, a Simscape Multibody model of the antagonistic triad and control system was created in MATLAB/Simulink. Plots of a test joint trajectory can be seen in figure 4.

A. TSA State Space Definition

In order to approximate a TSA plant from within a simulation, a state space model was required which takes motor current u as an input and outputs y as the TSA tension force f_i. [4] defines it as such, where J is the motor inertia, C is the motor coulomb friction (modified from viscous friction as the 1724TSR only has dry friction),, K_t is the motor torque constant, and K_L is the load stiffness. As the original definition is for a fixed load l_u distance from the motor a modified model is required which takes into account the varying length between the motor and load defined by $\Lambda(\boldsymbol{\theta})$. A saturation function is used to prevent incorrect compression forces when the string is slack. All of the motor coefficients were taken from the Faulhaber 1724TSR datasheet as this is the motor to be used in the experimental model. An estimated value is used for the load stiffness, this was chosen to be a high number as the model is expected to be very stiff.

$$\begin{aligned} h(\theta_s) &= \frac{\theta r_s^2}{\sqrt{l_u^2 - \theta_s^2 r_s^2}} \\ k(\theta_s, \boldsymbol{\theta}) &= \lambda_n(\boldsymbol{\theta}) - \sqrt{l_u^2 - \theta_s^2 r_s^2} \\ \dot{\boldsymbol{x}} &= \begin{bmatrix} x_2 \\ -\frac{K_L}{J} h(x_1)\, k(x_1, \boldsymbol{\theta}) - \frac{B}{J}\operatorname{sgn}(x_2) \end{bmatrix} + \begin{bmatrix} 0 \\ \frac{K_t}{J} \end{bmatrix} u \\ y &= K_L \operatorname{sat}_0^{\infty} k(x_1, \boldsymbol{\theta}) \end{aligned} \tag{18}$$

The state space model was then adapted to include constraints on motor velocity and acceleration set by the motor controller in order to keep the motor within design limits, by replacing $\dot{\boldsymbol{x}}$ with $\dot{\boldsymbol{x}}'$ which contains saturation functions for maximum motor velocity v_s and acceleration α_s.

$$\dot{\boldsymbol{x}}' = \begin{bmatrix} \operatorname{sat}_{\omega_s} \dot{x}_1 \\ \operatorname{sat}_{\alpha_s} \dot{x}_2 \end{bmatrix} \tag{19}$$

V. Performance Comparison

A. Tension Force and Stroke Velocity

The two most important performance metrics are the maximum tension force f_{max} and maximum stroke velocity $\dot{p}_{max}$. For both the TSA and leadscrew $f_{max} \propto \frac{1}{\dot{p}_{max}}$ holds true as the mutable coefficients are changed for the AUJ, so finding a balance between these two metrics is required. These are dependant on the maximum motor torque τ_{max} and motor velocity $\dot{\theta}_{max}$.

For the TSA metrics, the equations from [4], in particular $h(\theta)$ and $k(\theta)$ as used for the State Space in equation **??**, which can be used to determine f_{max} and $\dot{p}_{max}$ using equations **??** and **??**. By extracting coefficient r_s as an input to make $f(p, r_s)$ and $\dot{p}(\dot{\theta}, p, r_s)$ the performance of different string thicknesses can be compared for a given unwound length l_u and $\tau_{max}, \dot{\theta}_{max}$ over the range of the contraction length p.

For the leadscrew metrics, the raising torque calculation [] can be used as the absolute value of f_{max}, since the TSA only operates in tension, which can be used to determine the same metrics using equation **??**. The performance of different screw diameters d_m and leads λ can then be compared for a given τ_{max}. $\dot{p}_{max}$ is then simply calculated by multiplying λ with $\dot{\theta}_{max}$ converted from $\mathrm{rad\,s^{-1}}$ to $\mathrm{rev\,s^{-1}}$ to match the units of λ as in equation **??**. The performance of different λ can then be compared for a given $\dot{\theta}_{max}$.

$$
\begin{aligned}
k(\theta) &= l_u - \sqrt{l_u^2 - \theta_s^2 r_s^2} \\
k^{-1}(p) &= \pm \frac{\sqrt{p(2l_u - p)}}{r_s} \\
h^{-1}(\theta) &= \frac{\sqrt{l_n^2 - r_s^2\theta^2}}{r_s^2\theta} \\
f(p) &= h^{-1}\left(k^{-1}(p)\right) = \pm \frac{\sqrt{(l_u - p)^2}}{r_s\sqrt{p\,(2l_u - p)}} \\
f_{max} &= f(p)\tau_{max}
\end{aligned}
\tag{20}
$$

$$
\begin{aligned}
\dot{k}\left(\dot{\theta}, \theta\right) &= \frac{\dot{\theta} r_s^2 \theta}{\sqrt{l_n^2 - r_s^2\theta^2}} \\
\dot{p}\left(\dot{\theta}, p\right) &= \dot{k}\left(\dot{\theta}, k^{-1}(p)\right) = \pm \frac{\dot{\theta} r_s \sqrt{p\,(2l_n - p)}}{\sqrt{(l_n - p)^2}} \\
\dot{p}_{max} &= \dot{p}\left(\dot{\theta}_{max}, p\right)
\end{aligned}
\tag{21}
$$

$$
\begin{aligned}
|\tau(f)| &= \frac{d_m f\,(\lambda + \pi d_m \mu)}{2\,(\pi d_m - \lambda\mu)} \\
|f(\tau)| &= \frac{2\tau\,(\pi d_m - \lambda\mu)}{d_m\,(\lambda + \pi d_m \mu)} \\
f_{max} &= |f(\tau_{max})|
\end{aligned}
\tag{22}
$$

$$
\begin{aligned}
\dot{p}\left(\dot{\theta}\right) &= \lambda \frac{\dot{\theta}}{2\pi} \\
\dot{p}_{max} &= \dot{p}\left(\dot{\theta}_{max}\right)
\end{aligned}
\tag{23}
$$

As the values for τ_{max} and $\dot{\theta}_{max}$ for the TSA depend on p, but remain constant for the leadscrew, the performance of the TSA is going to be better or worse than a given leadscrew depending on the value p. Figure **??** compares the TSA configuration using the coefficients from table **??** against a number of common leadscrew configurations that are practical for the dimensions of the AUJ []. As can be noted, the TSA outperforms or underperforms different leadscrew configurations depending on p.

VI. Conclusion

Based on the current progress of research, Further refinements need to be made to the control system to ensure total stability within a significant joint range of the AUJ. An experimental model has also been constructed to validate the results from the simulation. In the longer term various performance metrics will be used to compare the TSA to alternative actuation methods.

References

[1] R. O. Buckingham and A. C. Graham, "Dexterous manipulators for nuclear inspection and maintenance — case study," in *2010 1st International Conference on Applied Robotics for the Power Industry*, 2010, pp. 1–6.

[2] M. Luo, R. Yan, Z. Wan, Y. Qin, J. Santoso, E. H. Skorina, and C. D. Onal, "Orisnake: Design, fabrication, and experimental analysis of a 3-d origami snake robot," *IEEE Robotics and Automation Letters*, vol. 3, no. 3, pp. 1993–1999, 2018.

[3] W. S. Rone, W. Saab, and P. Ben-Tzvi, "Design, Modeling, and Integration of a Flexible Universal Spatial Robotic Tail," *Journal of Mechanisms and Robotics*, vol. 10, no. 4, 04 2018, 041001. [Online]. Available: https://doi.org/10.1115/1.4039500

[4] T. Würtz, C. May, B. Holz, C. Natale, G. Palli, and C. Melchiorri, "The twisted string actuation system: Modeling and control," in *2010 IEEE/ASME International Conference on Advanced Intelligent Mechatronics*, July 2010, pp. 1215–1220.

[5] F. Dessen, "Coordinating control of a two degrees of freedom universal joint structure driven by three servos," in *Proceedings. 1986 IEEE International Conference on Robotics and Automation*, vol. 3, April 1986, pp. 817–822.

Damian J. Crosby is a PhD student in the school of Mechanical, Aerospace and Civil Engineering, University of Manchester, Manchester, U.K. He received a B.Sc. in Special Effects Development from The University of Bolton, U.K., in 2010, and a M.Res. in Robotics from The University of Plymouth, U.K., in 2012. He worked as a Research Technician at The University of Manchester from 2013 to 2017, before commencing his PhD.

Joaquin Carrasco is a Lecturer at the School of Electrical and Electronic Engineering, University of Manchester, UK. He was born in Abarn, Spain, in 1978. He received the B.Sc. degree in physics and the Ph.D. degree in control engineering from the University of Murcia, Murcia, Spain, in 2004 and 2009, respectively. From 2009 to 2010, he was with the Institute of Measurement and Automatic Control, Leibniz Universitt Hannover, Hannover, Germany. From 2010 to 2011, he was a research associate at the Control Systems Centre, School of Electrical and Electronic Engineering, University of Manchester, UK.

William P. Heath is Chair of Feedback and Control in the School of Electrical and Electronic Engineering, University of Manchester, Manchester, U.K. He received the B.A. and M.A. degrees in mathematics from Cambridge University, U.K., in 1987 and 1991, and the M.Sc. and Ph.D. degrees in systems and control from the University of Manchester Institute of Science and Technology, U.K., in 1989 and 1992, respectively. He was with Lucas Automotive from 1995 to 1998 and was a Research Academic at the University of Newcastle, Australia from 1998 to 2004. His research interests include absolute stability, multiplier theory, constrained control, and system identification.

Dr. Andrew Weightman graduated in 2006 with a PhD in Mechanical Engineering form the University of Leeds. Whilst at the University of Leeds he developed rehabilitation robotic technology for improving upper limb function in adults and children with neurological impairment which was successfully utilised in homes, schools and clinical settings. In 2013 he moved to the University of Manchester, School of Mechanical, Aerospace and Civil Engineering as a Lecturer in Medical Mechatronics. Dr Weightman has research interests in biomimetic mobile robotics, rehabilitation robotics, robotics for nuclear decommissioning and collaborative robotics.

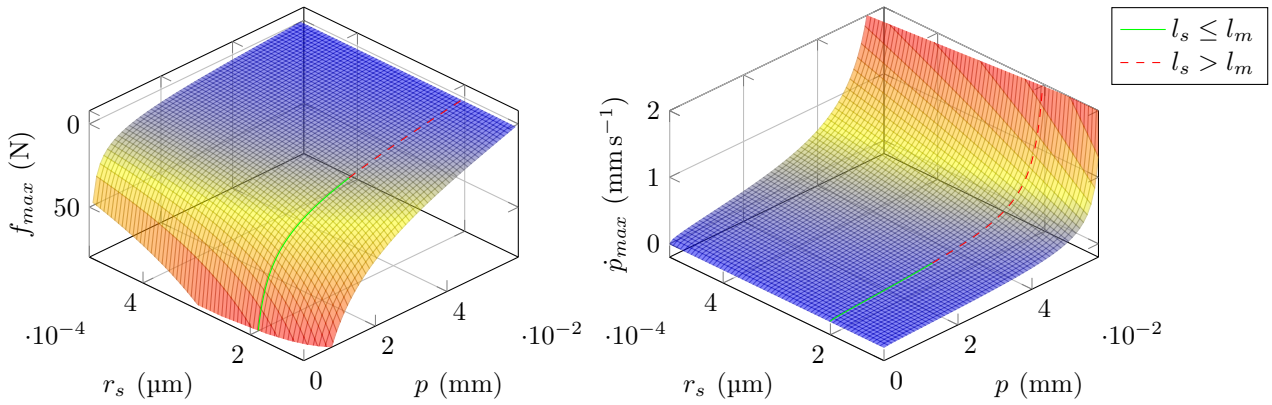

Fig. 5

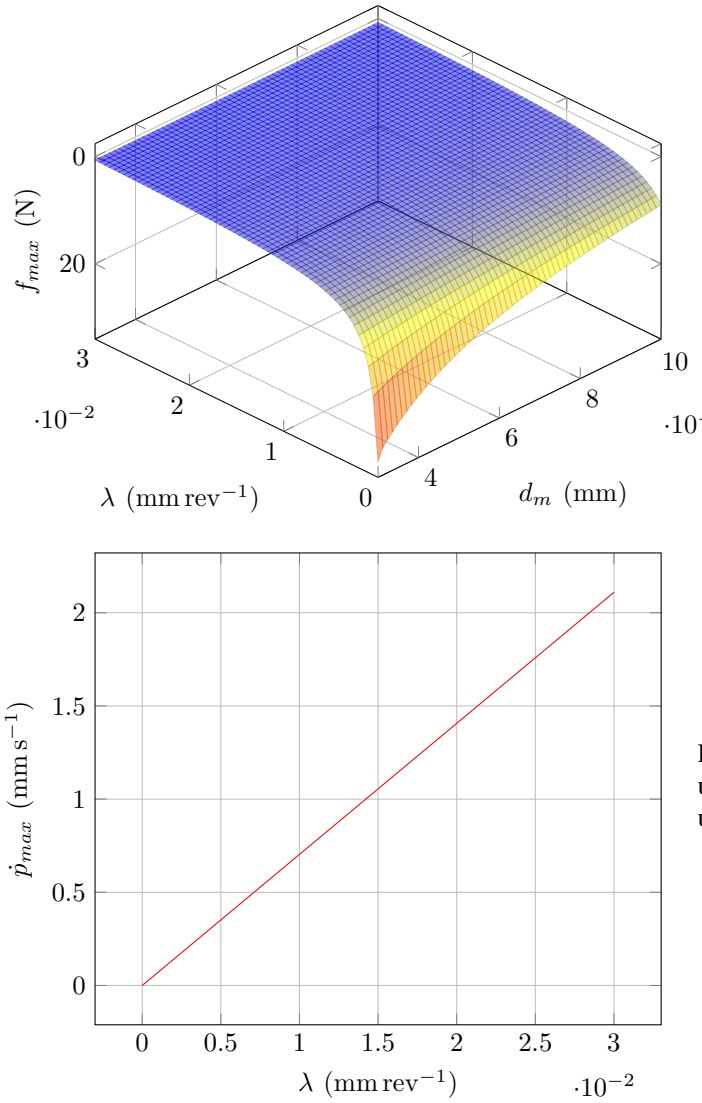

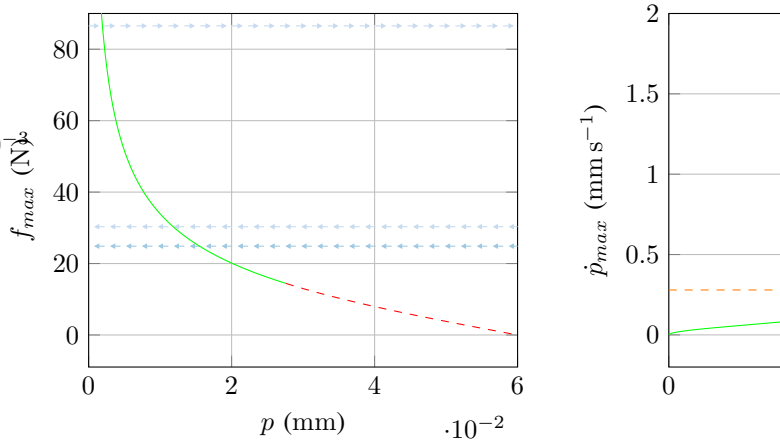

Fig. 6: Performance comparison of the TSA configuration using coefficients from table **??** to various leadscrew configurations with different d_m and λ.

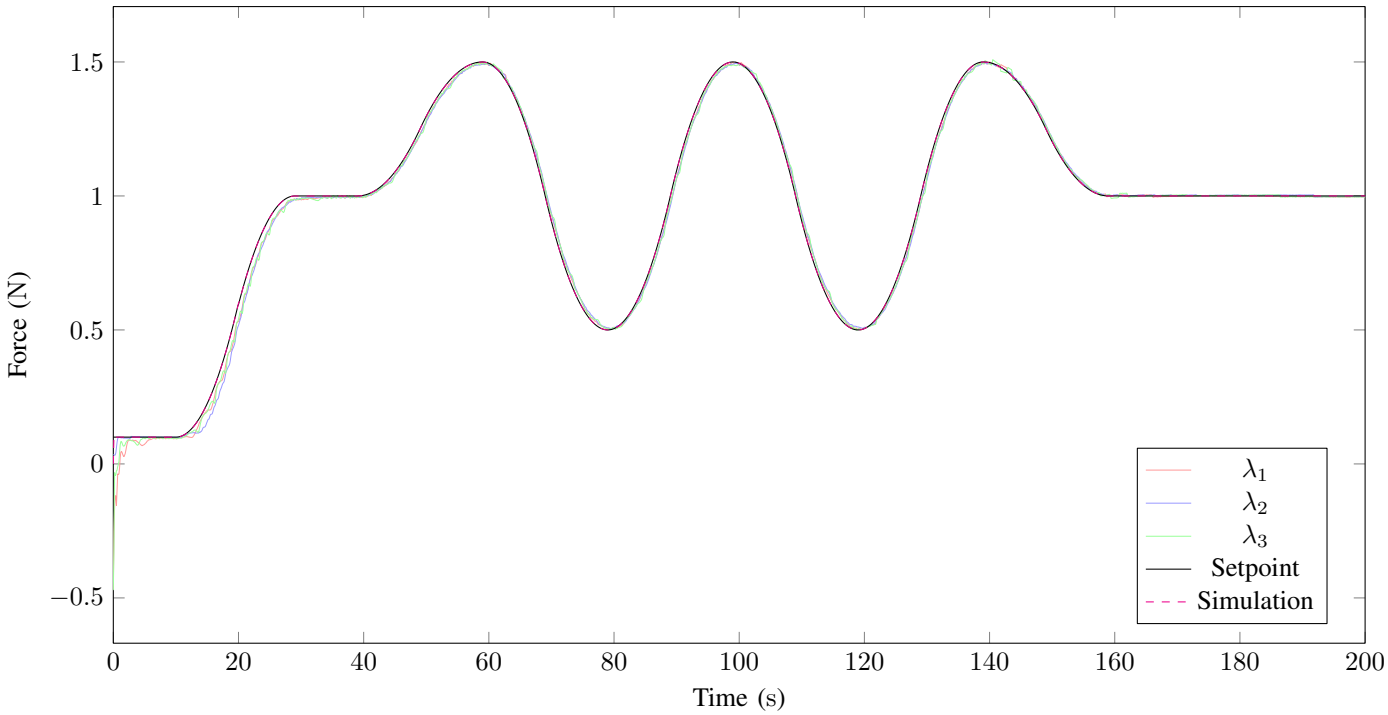
Force (N)
1.5
1
0.5
0
−0.5
0
20
40
60
80
100
120
140
160
180
200
Time (s)
λ_1
λ_2
λ_3
Setpoint
Simulation

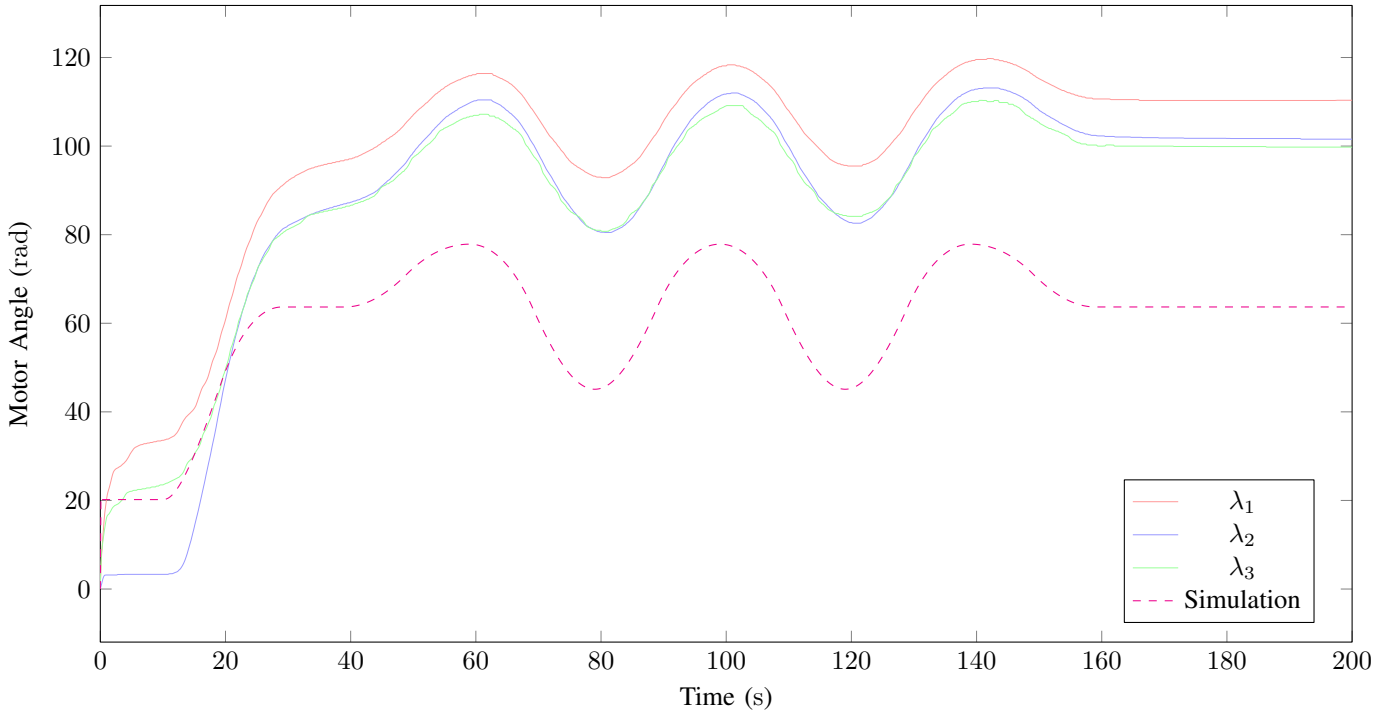
Motor Angle (rad)
120
100
80
60
40
20
0
0
20
40
60
80
100
120
140
160
180
200
Time (s)
λ_1
λ_2
λ_3
Simulation

Fig. 7

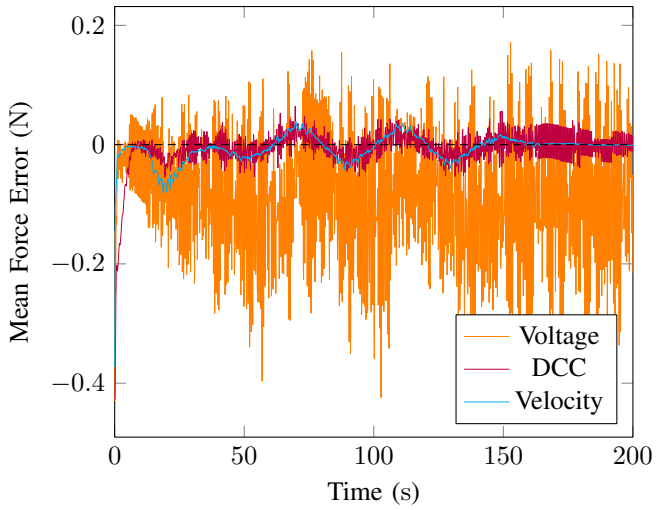
0.2
0
−0.2
−0.4
Mean Force Error (N)
0
50
100
150
200
Time (s)
Voltage
DCC
Velocity

Fig. 8

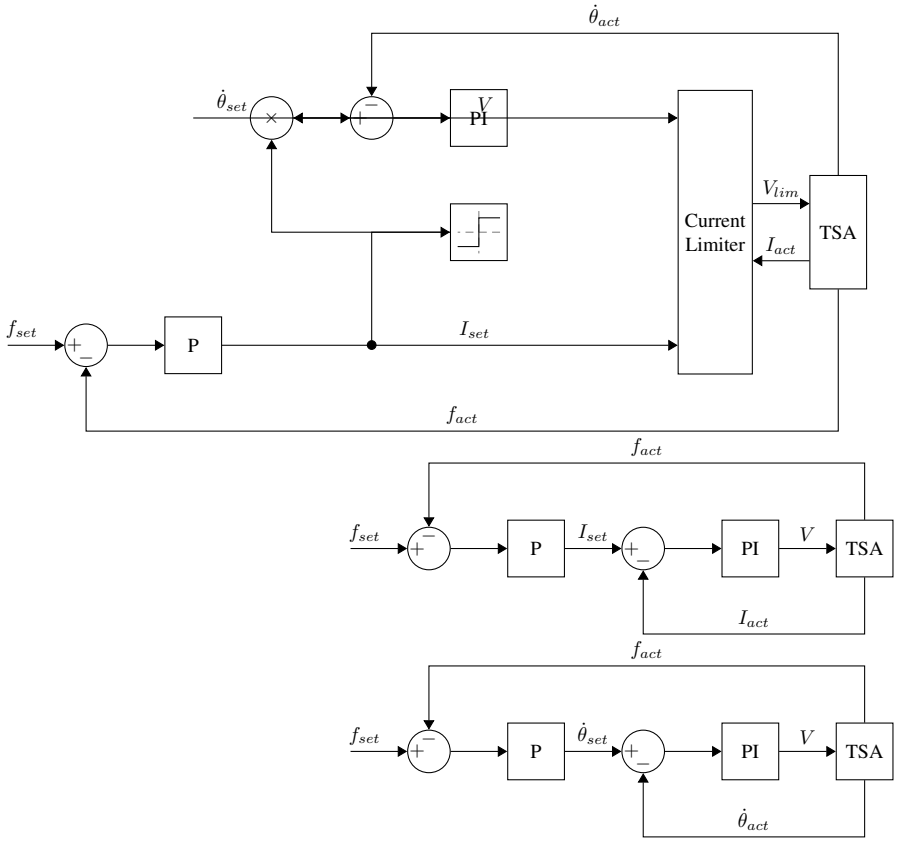
$\dot{\theta}_{act}$
$\dot{\theta}_{set}$
PI
V
Current Limiter
V_{lim}
I_{act}
TSA
f_{set}
P
I_{set}
f_{act}
f_{act}
f_{set}
P
I_{set}
PI
V
TSA
I_{act}
f_{act}
f_{set}
P
$\dot{\theta}_{set}$
PI
V
TSA
$\dot{\theta}_{act}$